

# Mitotic Rounding Alters Cell Geometry to Ensure Efficient Bipolar Spindle Formation

Oscar M. Lancaster,<sup>1,6</sup> Maël Le Berre,<sup>5,6</sup> Andrea Dimitracopoulos,<sup>1,4</sup> Daria Bonazzi,<sup>5</sup> Ewa Zlotek-Zlotkiewicz,<sup>5</sup> Remigio Picone,<sup>1,4</sup> Thomas Duke,<sup>2,3</sup> Matthieu Piel,<sup>5,\*</sup> and Buzz Baum<sup>1,\*</sup>

<sup>1</sup>MRC Laboratory for Molecular Cell Biology

<sup>2</sup>London Centre for Nanotechnology

<sup>3</sup>Department of Physics and Astronomy

<sup>4</sup>CoMPLEX

University College London, Gower Street, London WC1E 6BT, UK

<sup>5</sup>Systems Biology of Cell Division and Cell Polarity, UMR 144 Institut Curie/CNRS, 26 rue d'Ulm, 75248 Paris Cedex 05, France

<sup>6</sup>These two authors contributed equally to this work

\*Correspondence: [matthieu.piel@curie.fr](mailto:matthieu.piel@curie.fr) (M.P.), [b.baum@ucl.ac.uk](mailto:b.baum@ucl.ac.uk) (B.B.)

<http://dx.doi.org/10.1016/j.devcel.2013.03.014>

## SUMMARY

Accurate animal cell division requires precise coordination of changes in the structure of the microtubule-based spindle and the actin-based cell cortex. Here, we use a series of perturbation experiments to dissect the relative roles of actin, cortical mechanics, and cell shape in spindle formation. We find that, whereas the actin cortex is largely dispensable for rounding and timely mitotic progression in isolated cells, it is needed to drive rounding to enable unperturbed spindle morphogenesis under conditions of confinement. Using different methods to limit mitotic cell height, we show that a failure to round up causes defects in spindle assembly, pole splitting, and a delay in mitotic progression. These defects can be rescued by increasing microtubule lengths and therefore appear to be a direct consequence of the limited reach of mitotic centrosome-nucleated microtubules. These findings help to explain why most animal cells round up as they enter mitosis.

## INTRODUCTION

The microtubule and actin cytoskeletons act together to give animal cells their dynamic form. As cells enter mitosis, these two cytoskeletal systems undergo rapid remodeling to perform distinct functions. For the microtubule cytoskeleton (Walczak and Heald, 2008), this process begins as cells enter mitosis with the disassembly of interphase microtubules and the nucleation of a population of shorter, dynamic microtubules from centrosomes that, following nuclear envelope breakdown (NEB), establish contacts with chromosomes and form antiparallel microtubule bundles. This leads to the assembly of a bipolar spindle (Magidson et al., 2011). Captured chromosomes are then brought to the spindle midzone to form a metaphase plate (Magidson et al., 2011). Finally, once all kinetochores are properly bioriented and the spindle assembly checkpoint (SAC) is satisfied, cells enter anaphase, triggering a loss of sister-

chromatid cohesion and the movement of sister chromatids to opposite cell poles.

Mitotic progression is also accompanied by profound changes in actin filament organization (Kunda and Baum, 2009) that are triggered by the activation of Ect2, RhoA, and Myosin II (Cramer and Mitchison, 1997; Maddox and Burridge, 2003; Matthews et al., 2012). In combination with osmotic swelling (Stewart et al., 2011) and the disassembly of stress fibers and focal contacts (Dao et al., 2009), the actin-dependent forces generated are sufficient to drive mitotic rounding. Concurrently, ERM proteins are activated, crosslinking actin filaments to the overlying plasma membrane to generate a stiffened metaphase cortex (Carreno et al., 2008; Kunda et al., 2008). Then, at anaphase, the actin cytoskeleton is remodeled through the generation of a contractile ring (Fededa and Gerlich, 2012) and relaxation of the cortex at cell poles (Kunda et al., 2012; Sedzinski et al., 2011), driving cell division.

Although the major changes in the organization and dynamics of the actin and microtubule cytoskeletons appear to be largely independent at the onset of mitosis (Matthews et al., 2012), there is evidence for specific modes of crosstalk between the spindle and the mitotic cortex. Actomyosin cortical flows early in mitosis are thought to aid centrosome separation (Rosenblatt et al., 2004), and polarized cues embedded in the actin cortex activate Dynein-based pulling forces to guide spindle positioning and alignment (Morin and Bellaïche, 2011). This process of spindle positioning in turn influences the actin cortex by governing the position of the actomyosin ring at cytokinesis, as microtubule plus ends overlapping at the midzone of the anaphase spindle recruit the centralspindlin complex, activating Rho to trigger localized actomyosin assembly and contractile furrow formation (Fededa and Gerlich, 2012). There have also been various reports of actin and actin-binding proteins functioning at the heart of the spindle (Sandquist et al., 2011), and several groups have observed defects in spindle formation following perturbations of the actin cytoskeleton (Kunda et al., 2008; Luxenburg et al., 2011). Such observations suggested the possibility that the actin cytoskeleton might play a direct role in spindle formation itself (Sandquist et al., 2011; Tse et al., 2012; Vilmos et al., 2009).

Here, we test this idea using a combination of molecular genetic tools and micromanipulation to dissect the relative roles

of actin filaments, cortical rigidity, and cell shape in spindle morphogenesis. Our analysis reveals that the actin cytoskeleton contributes little to spindle morphogenesis in isolated HeLa cells but is essential in cells under conditions of confinement, where it is required to drive mitotic rounding—a process that is vital for efficient and stable bipolar spindle formation. Together, these findings help to explain the near-ubiquitous concurrence of spindle assembly and mitotic rounding in proliferating animal cells.

## RESULTS

### Rounding Is Required for Timely Mitotic Progression

Although rounding is a striking feature of mitosis in most proliferating cells that lack a cell wall (ranging from *Dictyostelium* to metazoan cells in isolation and in tissues; Gibson et al., 2011), its function remains obscure. To determine the role of mitotic rounding, we used changes in adhesion (Dao et al., 2009) and physical confinement (Dumont and Mitchison, 2009; Le Berre et al., 2012) to precisely modulate the geometry of cells in culture as they enter mitosis (Figure 1A).

We monitored rounding in HeLa cells expressing a constitutively activated version of the small GTPase Rap1 (here called Rap1<sup>\*</sup>; Figure 1A). Previously, endogenous Rap1 activity was shown to be downregulated in mammalian cells entering mitosis (Dao et al., 2009), and Rap1<sup>\*</sup> expression was shown to block adhesion disassembly and retraction of the cell margin during mitotic rounding (Dao et al., 2009; Figure 1D). In line with this, we found that although control HeLa cells rounded up within ~18 min of entering mitosis, concomitantly reducing their spread area and increasing their height (from 7  $\mu\text{m}$  in G2 to ~20  $\mu\text{m}$  at metaphase) to form near-perfect spheres, Rap1<sup>\*</sup>-expressing cells remained well spread throughout mitosis (Figures 1B, 1D, and 1E). This constitutive spreading limited the rounding of Rap1<sup>\*</sup> cells entering mitosis to ~5–6  $\mu\text{m}$  in height at NEB (Figure 1B), rising to ~9–10  $\mu\text{m}$  at metaphase (Figures 1D and 1E), and visibly constrained the height of the metaphase plate (Figure 1D; Figure S1A available online). This inhibition of mitotic rounding was associated with a significant delay in mitotic progression, measured as the time from NEB to anaphase (Figure 1C). This effect was reversed both by RNA interference (RNAi)-mediated silencing of the adhesion complex component Talin, which prevented Rap1<sup>\*</sup>-induced cell spreading (Figures S1B and S1C), and by increasing the density of Rap1<sup>\*</sup> cells to reduce their spread area at the onset of mitosis (Figures S1D–S1F).

To determine more precisely how Rap1<sup>\*</sup>-induced changes in cell geometry affect mitotic progression, we used micropatterned adhesive islands with different shapes to independently modify the height and spread area of Rap1<sup>\*</sup> cells (Figure 1D). When Rap1<sup>\*</sup> cells were plated on large oval micropatterns, they remained flat throughout mitosis and mitotic progression was delayed (Figures 1E and 1F). However, normal mitotic timing was restored in cells on small adhesive oval micropatterns (Figure 1F), which reached a height of ~13–14  $\mu\text{m}$  at metaphase (Figure 1E), equivalent to the height of the metaphase plate in rounded control cells (Figure S1A). As a further test of the role of cell shape in mitotic progression, we placed polyacrylamide hydrogels of calibrated stiffness above cells in interphase, so that cells were forced to deform the gel to round up upon entry into mitosis (Figure 1A). By gradually increasing the stiffness of

this external barrier, we were then able to progressively limit mitotic rounding (Figures 1G and 1H). Hydrogels between 3 and 15 kPa in stiffness limited metaphase cell height to ~8–11  $\mu\text{m}$  (inferred from measurements of cell diameter; Figure 1H), a value similar to that seen in metaphase Rap1<sup>\*</sup> cells (Figure 1E). Under these conditions, the time between NEB and anaphase onset was increased ~2-fold (Figure 1I), similar to what was seen in Rap1<sup>\*</sup> cells. This delay was lengthened as gel stiffness was increased to 20 and 30 kPa to further limit mitotic rounding (Figure 1I). Having established that Rap1<sup>\*</sup> expression and stiff hydrogels delay mitotic progression by limiting mitotic cell rounding, we also tested the effects of imposing a fixed height on cells with a rigid polydimethylsiloxane (PDMS)-coated glass slide (Figures 1A and 1G; Le Berre et al., 2012). By systematically lowering this fixed roof from 8 to 5  $\mu\text{m}$ , we found that the time from NEB to anaphase was progressively increased once heights were reduced to  $\leq 7$   $\mu\text{m}$  (Figure 1I)—heights that are equivalent in range to those of Rap1<sup>\*</sup> cells at NEB.

In each of these treatments used to flatten mitotic cells, reductions in cell height were accompanied by varying extents by corresponding increases in cell width. It was therefore important to separate these two parameters to determine their relative impact on mitosis. To do so, we plated HeLa cells expressing Rap1<sup>\*</sup> on micropatterned lines to generate mitotic cells with a long axis and a height of ~13–14  $\mu\text{m}$  (Figures 1D and 1E), equivalent to the average unconstrained height of the metaphase plate in control HeLa cells (Figure S1A). Significantly, this rescued mitotic timing (Figure 1F), implying that it is the limit in cell height (the smallest cell dimension), not the change in width, that delays mitotic progression in flattened cells. Taken together, these data confirm the importance of cell rounding and its associated changes in cell geometry for timely mitotic progression.

### Flat Mitotic Cells Are Defective in Chromosome Capture

Delays in mitotic progression are often associated with spindle defects and induction of the SAC (Musacchio, 2011). In line with this, the mitotic delay observed in Rap1<sup>\*</sup> cells and in cells confined to a height of 5  $\mu\text{m}$  was eliminated when the checkpoint was silenced using *MAD2* small interfering RNAs (siRNAs; Figures S2A and S2B), implicating spindle defects in the mitotic delay. Previous work observed changes in spindle architecture (Dumont and Mitchison, 2009) and defects in division (Tse et al., 2012) following mitotic cell compression. So, to determine whether cell geometry influences spindle formation in flat HeLa cells, we analyzed the path of spindle assembly using histone-2B-mCherry and  $\alpha$ -tubulin-GFP in cells constrained in height by the expression of Rap1<sup>\*</sup> or through 5  $\mu\text{m}$  physical confinement. Nuclei were flattened in these cells as they entered mitosis. As a result, the chromosomes that were released upon NEB became arrayed over a relatively large area (Figures 2A and 2B), which prevented many of them from establishing early contacts with microtubules emanating from the two centrosomes. This led to the loss of chromosomes from the nascent spindle (Figures 2A and 2B, yellow arrows; control: 0% [n = 47]; Rap1<sup>\*</sup>: 31% [n = 54]). Furthermore, chromosomes in flattened cells frequently became arrayed around centrosomes and along the sides of newly forming bipolar spindles (Figures 2A and 2B, blue arrows; control: 25% [n = 48]; Rap1<sup>\*</sup>: 79% [n = 53]) before congressing to the spindle midzone. Anaphase

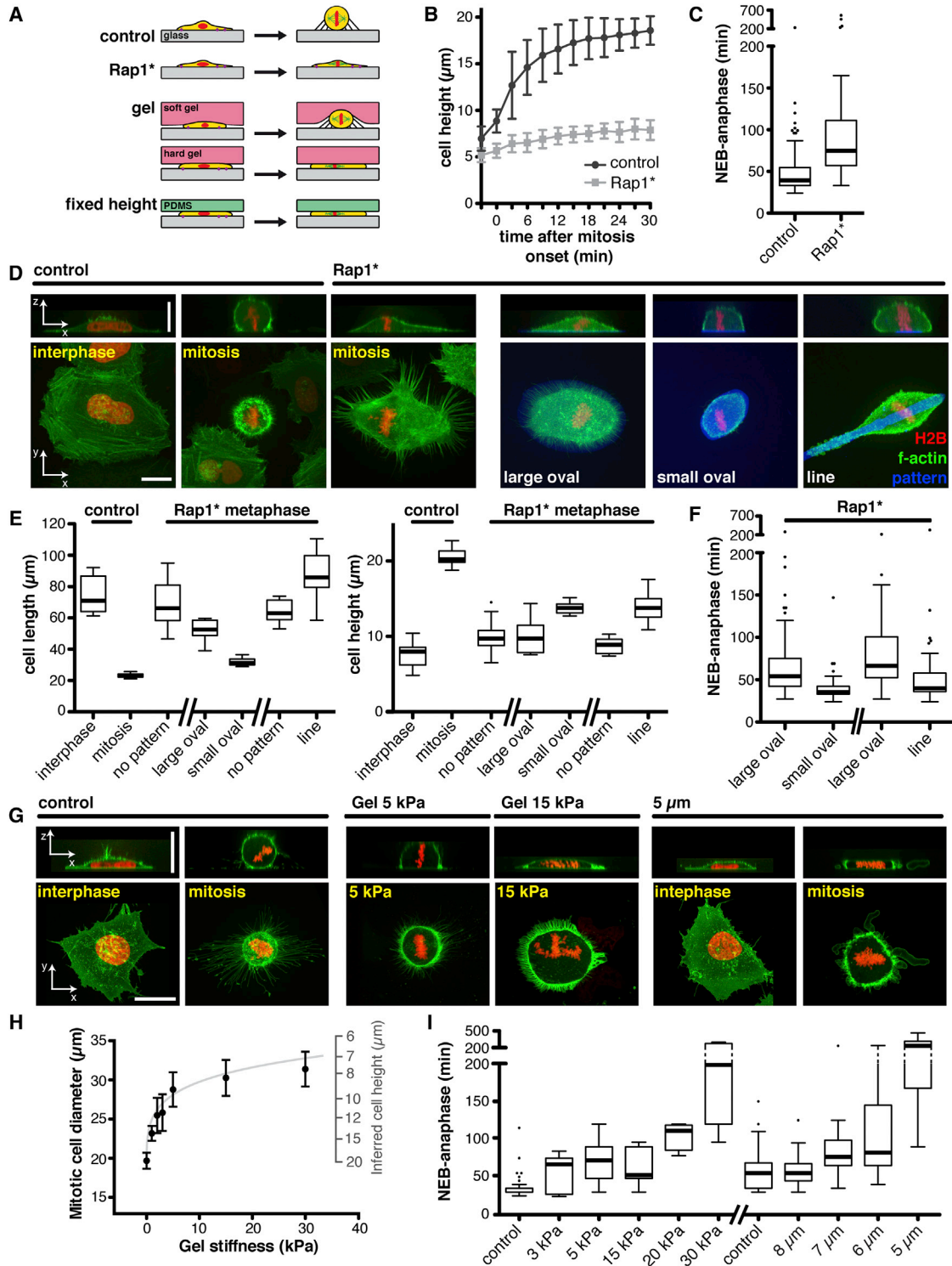


**Figure 1. A Failure in Cell Rounding Delays Mitotic Progression**

(A) Schematic diagram showing the different methods we used to perturb mitotic cell rounding.

(B) Heights of control (n = 8) and Rap1\* (n = 7) cells as the cells entered mitosis. Means and SD from the mean are shown.

(C) Times from NEB to anaphase for control (n = 86) and Rap1\*-expressing cells (n = 52). Rap1\*-expressing cells exhibited a near 2-fold delay in anaphase onset timing (p < 0.001, unpaired t test).

(D) Representative x-y (maximum projection) and x-z (single plane) confocal images of control and Rap1\* cells in interphase and at metaphase on unpatterned and patterned substrates.

(E) Maximum length and height of the cells described in (D) (n ≥ 8).

(legend continued on next page)

onset was then initiated after visible completion of the metaphase plate (Figures 2A and 2B).

To assess whether the defects in early chromosome capture in flattened cells contributed to the observed delay in mitotic progression, we measured the rate of chromosome “gathering” (Figure 2C), expressed as a fractional change in the nuclear area (Figure 2C). For each cell, we fitted these data to a parametric model,  $y = 1 - C(1 - \exp(-kt))$ , where  $C$  is the total relative decrease in chromosome area and  $k$  is the rate of decrease (Figure 2D). Because the  $R^2$  values indicated a good fit with the data (Figure 2D, inset), we were able to extract the parameters  $C$  and  $k$  for all cells in populations of rounded and flat mitotic cells. Although there was no significant difference in the extent of chromosome gathering (Figure 2E), the decrease in  $k$  (median values for  $k$ : control, 0.16; Rap1\*, 0.09;  $p < 0.01$ , unpaired t test) revealed a near 2-fold reduction in the rate at which chromosomes were gathered in flattened Rap1\* cells (Figure 2E), helping to explain the accompanying near 2-fold delay in the time required to form a metaphase plate (Figure 1C).

### The Reach of Astral Microtubules and Chromosome Distribution at NEB Determine the Rate of Chromosome Capture

To better understand the cause of the observed defects in chromosomal capture, we next turned our attention to astral microtubules. Although astral microtubules appeared significantly longer in fixed Rap1\* cells when compared with the corresponding control (Figure 3A and S3A), they rarely extended beyond  $\sim 15 \mu\text{m}$  as previously observed (Collins et al., 2012; Lénárt et al., 2005; Piehl and Cassimeris, 2003). This reinforces the well-established idea that microtubules have a delimited length (Varga et al., 2009; Picone et al., 2010) and do not perfectly scale with cell width (Collins et al., 2012; Wühr et al., 2008). As a result, few astral microtubules reached the distant edge of flattened cells (Figure S3B).

To test whether this limit in microtubule lengths could explain the reduced efficiency of chromosome capture in flat mitotic cells, we used the observed distribution to predict the likelihood that a given chromosome would lie within reach of centrosome-nucleated microtubules immediately following NEB (Figures 3B and 3C). It was clear from this analysis of Rap1\* cells at NEB that many chromosomes fall outside the predicted range of centrosomal microtubules (Figure 3E). This is best seen in spatial maps that represent the probability of centrosome-nucleated microtubules reaching a specific region of chromatin in control and Rap1\* cells (Figure 3C, grayscale images). By following these cells through the early stages of spindle assembly, we observed chromosomes being lost from the nascent spindle in Rap1\* cells

(Figure 3C, yellow arrows, and 3F) in regions least likely to be within the reach of microtubules at NEB (Figure 3C, grayscale images, yellow arrows). Thus, the altered geometric arrangement of chromosomes and microtubules in flat mitotic cells is sufficient to explain the observed defects in chromosome capture. In support of this idea, there was a further increase in the rate of chromosome loss in Rap1\* cells entering mitosis with centrosomes on the same side of the nucleus, as predicted using the same microtubule length distribution (Figure 3D, yellow arrow). By considering each centrosome separately, we were also able to use our microtubule length distribution to predict whether a given chromosome would fall within the range of microtubules emanating from one or both poles of the forming spindle (Figure 3C, color-coded images). Many more chromosomes fell outside the range of microtubules emanating from one of the two centrosomes in Rap1\* cells (Figure 3G). Instead of being rapidly moved to the metaphase plate, these chromosomes became arrayed around a single centrosome and gathered along the sides of the developing bipolar spindle (Figure 3C, blue arrows).

Using the SAC proteins Mad1 and BubR1, we were able to visualize defects in the attachment of chromosomes to the nascent spindle in fixed prometaphase Rap1\* cells. These proteins accumulated at the kinetochores of lost chromosomes (Figures S3C and S3D, blue arrows; Lara-Gonzalez et al., 2012). In addition, kinetochores on chromosomes arrayed along the sides of the nascent spindle were enriched in BubR1 (Figure S3D, yellow arrows; Skoufias et al., 2001; O’Connell et al., 2008) and exhibited syntelic microtubule attachments (Figure S3E). Because it takes time for such defects to be resolved, these findings help to explain the decrease in the rate of chromosome congression and the delay in anaphase onset in flat mitotic cells.

### The Limited Reach of Microtubules Leads to Pole Splitting in Flattened Mitotic Cells

Having established that limits in astral microtubule reach contribute to defects in spindle assembly, chromosome capture, and congression in mitotic cells that are unable to round up, we explored the effects of systematically reducing cell height on spindle architecture (Figure 4A). Consistent with previous studies (Dumont and Mitchison, 2009), we found that preventing rounding either by expressing Rap1\* or by physically limiting cell height led to an increase in the pole-to-pole length of metaphase spindles (Figure S4A; note that limiting mitotic rounding is not the same as actively flattening cells). Although we did not observe obvious defects in the structure of elongated spindles confined to a fixed height of  $8 \mu\text{m}$ , or in cells induced to flatten by growth under moderately stiff gels of 3–15 kPa or by the

(F) NEB to anaphase timing for Rap1\*-expressing cells on large ovals ( $n = 56$ ) versus small ovals ( $n = 35$ ), and large ovals ( $n = 85$ ) versus lines ( $n = 46$ ). The time to anaphase onset was significantly increased on large ovals ( $p < 0.01$ , unpaired t test).

(G) Representative x-y and x-z images of control cells, cells growing under gels of intermediate (5 kPa) and higher (15 kPa) stiffness, and cells at  $5 \mu\text{m}$  confinement.

(H) Diameter of mitotic cells as a function of gel stiffness. Means and SD from the mean are shown ( $n = 23, 19, 17, 47, 53, 17, 21$ ). The height of the cells was estimated from the cell diameter assuming an ellipsoid cell geometry. The gray line is a fit from a mechanical model (see Experimental Procedures).

(I) NEB-to-anaphase timing for control cells, cells growing under gels of increasing stiffness, and cells confined to a height of 8, 7, 6, or  $5 \mu\text{m}$  ( $n = 44, 9, 35, 15, 4, 4, 24, 21, 24, 38, 18$ ). At all levels of confinement, except  $8 \mu\text{m}$  ( $p = 0.89$ , unpaired t test), the time to anaphase onset was increased ( $p < 0.01$ , unpaired t test). Scale bars represent  $20 \mu\text{m}$ .

See also Figure S1.

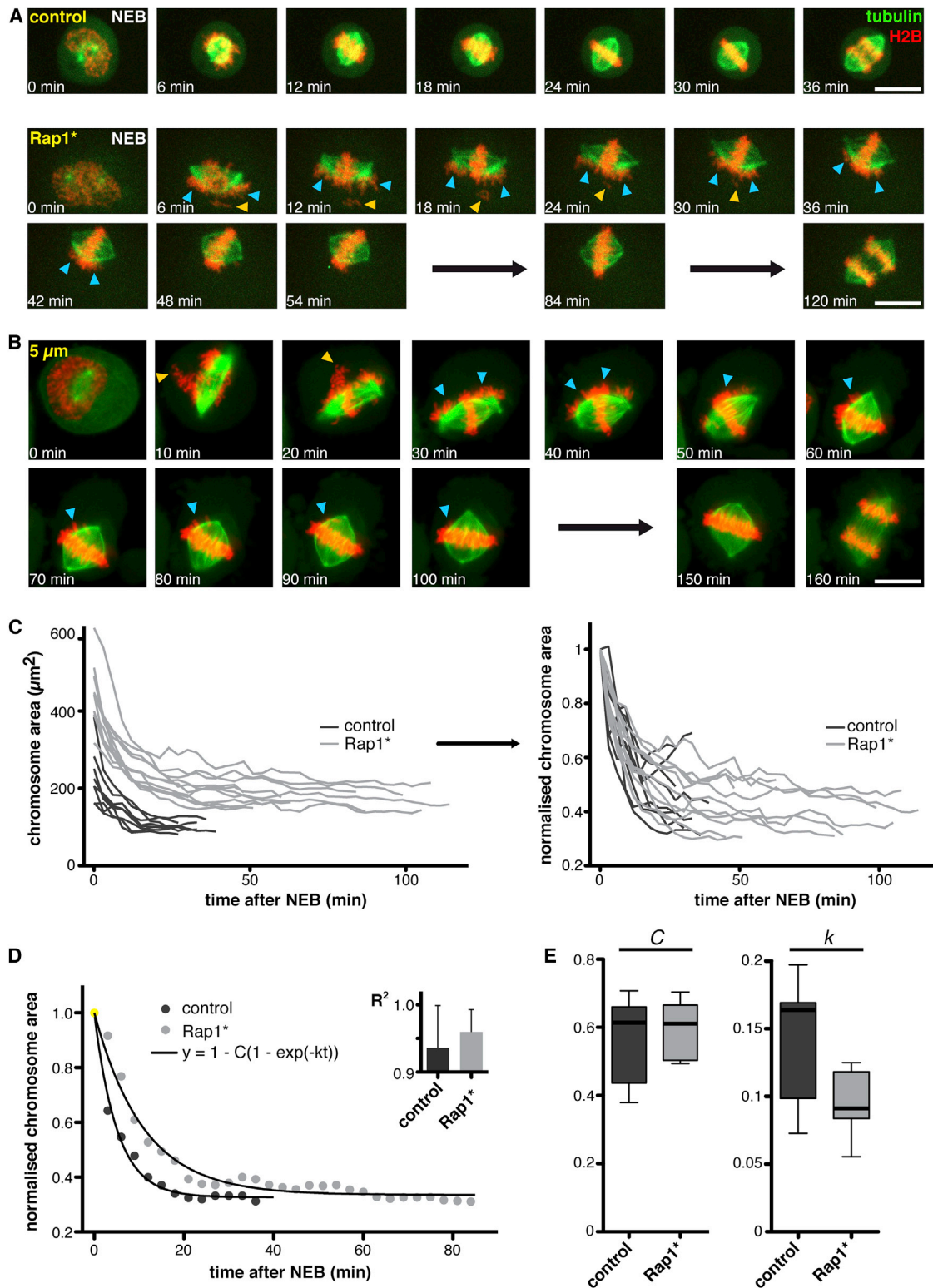


**Figure 2. Flat Mitotic Cells Are Defective in Chromosome Capture**

(A) Mitotic spindle formation in control and Rap1<sup>+</sup>-expressing HeLa cells. Representative time-lapse maximum projection images are shown (see also Movie S1). In flattened Rap1<sup>+</sup>-expressing cells, chromosomes were lost from the nascent spindle (yellow arrows) or became arrayed along the side of the forming spindle (blue arrows).

(B) Mitotic spindle formation in HeLa cells confined to 5  $\mu\text{m}$  in height. Representative time-lapse maximum projection images are shown (see also Movie S2).

(legend continued on next page)

expression of Rap1\*, a large proportion of profoundly flattened cells developed multipolar spindles (reaching ~60% at 5  $\mu\text{m}$ ) when gel stiffness was further increased or when fixed cell height was reduced below 8  $\mu\text{m}$  (Figures 4A and 4C). Moreover, below 5  $\mu\text{m}$ , a height at which both interphase and mitotic cells are physically confined, mitotic chromosomes were frequently seen spread around the two centrosomes, out of the reach of microtubules emanating from the opposite spindle pole. These chromosomes failed to congress to form a metaphase plate (Figures 4A and 4C), consistent with our proposal that limits to astral microtubule length and the increased chromosome spread in flat mitotic cells combine to perturb efficient chromosome capture. As a consequence, such cells underwent mitotic slippage, chromosome missegregation, and/or mitotic cell death.

Imaging spindles in mitotic cells confined to <8  $\mu\text{m}$  in height revealed that the ectopic poles generated by pole splitting (Figure 4B) lacked centrioles (Figure S4B). To investigate whether limits to microtubule reach might contribute to this type of pole splitting, we estimated the length of the longest spindle microtubules making chromosome attachments by measuring the distance from spindle poles to the farthest point on mitotic chromosomes (Figure 4B, dashed white line, and 4D). Pole-to-chromosome distances were found to be longer in cells dividing at fixed heights of 5 and 3.5  $\mu\text{m}$  when compared with the control (Figure 4D), as a result of the widening of the metaphase plate induced by the reduction in cell height (Figures S4C and S4D; Dumont and Mitchison, 2009). Again, these distances approached the limit in astral microtubule lengths measured above (~15  $\mu\text{m}$ ; Figure 3B). As the spindle grew to reach this critical length during the formation of a metaphase plate under confinement, we frequently observed spindle poles splitting to generate multipolar spindles that spread metaphase chromosomes between small subplates (Figures 4B, 4D, S4C, and S4D). This dramatically reduced the effective pole-to-chromosome distances within the spindle (Figures 4B, 4D, and S4C), bringing the chromosomes into a stable configuration well within reach of the population of microtubules emanating from spindle poles. In most cases, pole splitting was irreversible, as previously shown (Logarinho et al., 2012), and led to a lethal multipolar division. Again, these observations support the existence of a limit to the effective distance over which microtubules act within the context of a mitotic cell. In flat cells, this causes delays in chromosome capture and pole splitting to form shorter multipolar spindles that can better accommodate microtubules of a typical length.

### Rescuing Chromosome Capture and Pole Splitting in Flat Mitotic Cells by Increasing Microtubule Lengths

If the mitotic defects observed in flat cells result from the limited reach of microtubules, it should be possible to rescue them by

increasing the microtubule lengths. To put this idea to the test, we used RNAi to deplete mitotic cells of centromere-associated kinesin (MCAK; Figure S5A), a microtubule-depolymerizing kinesin whose depletion from HeLa cells increases mitotic microtubule lengths (Domnitz et al., 2012). We detected a significant increase in astral microtubule lengths in monopolar spindles in MCAK-depleted Rap1\* cells generated using the small-molecule Eg5 kinesin inhibitor S-trityl-L-cysteine (STLC; Rap1\* control RNAi: mean length  $12.43 \pm 2.98 \mu\text{m}$  [n = 821]; Rap1\* MCAK RNAi: mean length  $14.58 \pm 3.48 \mu\text{m}$  [n = 626];  $p < 0.0001$ , unpaired t test). This translated into a moderate but significant increase in astral microtubule lengths emanating from centrosomes in the context of bipolar Rap1\* spindles (control RNAi: mean length  $10.24 \pm 4.13 \mu\text{m}$  [n = 405]; MCAK RNAi: mean length  $10.95 \pm 4.28 \mu\text{m}$  [n = 579];  $p = 0.0096$ , unpaired t test), and an increase in bipolar spindle length (Figure S5B; Domnitz et al., 2012). Significantly, this was sufficient to rescue defects in chromosome capture in flat mitotic cells. Thus, fewer chromosomes were lost from nascent spindles in MCAK-depleted Rap1\* cells during the earliest stages of spindle formation than in the corresponding control (Figures 5A and 5C). Strikingly, MCAK RNAi also rescued multipolar spindle formation in cells confined to 5  $\mu\text{m}$  in height (Figures 5B and 5D), leading to a significant reduction in the timing of anaphase onset (Figure S5C). These observations demonstrate that the defects in spindle assembly and pole stability seen in flat mitotic cells likely result from the limited reach of mitotic microtubules.

### Roles for Actin in Spindle Assembly

The above analysis suggests that geometric constraints limit the ability of cells that have failed to undergo mitotic rounding to form a functional bipolar spindle efficiently. How does the actin cytoskeleton contribute to these processes? The actin cytoskeleton is known to help generate the forces that drive mitotic rounding (Figure 6A; Maddox and Burridge, 2003) and has been proposed to play direct roles in spindle assembly (Sandquist et al., 2011; Tse et al., 2012; Vilmos et al., 2009). To determine the relative importance of these roles for actin in our system, we studied mitotic progression in cells in the presence or absence of the actin poison latrunculin B (lat B). Importantly for this analysis, the treatment both removes the bulk of actin filaments and causes isolated interphase cells to round up (Figure 6B). Although addition of lat B induced failure in cytokinesis, as expected following the loss of actin filaments (Figure 6B), the timing of anaphase onset in these rounded cells was similar to that observed in the control (Figure 6C). By contrast, a significant delay in anaphase onset was seen in control experiments in cells treated with a low dose of the microtubule inhibitor nocodazole (Figure 6C; Uchida et al., 2009). These

(C) Chromosome area as a function of time in control and Rap1\* cells (left graph: each line represents data from one cell). Chromosome area was expressed as a fraction of the initial area at NEB (right graph).

(D) Plots of normalized chromosome area against time were fitted to a parametric model,  $y = 1 - C(1 - \exp(-kt))$ , where  $C$  is the total relative decrease in chromosome area and  $k$  is the rate of decrease. A single representative data set with the fitted model (black line) is shown for control and Rap1\*-expressing cells. Mean  $R^2$  values for control (n = 8) and Rap1\* (n = 11) data sets are shown in the inserted bar graph. Error bars represent SD from the mean.

(E) Values of  $C$  and  $k$  for control (n = 8) and Rap1\*-expressing (n = 11) cells are plotted as a box-and-whiskers plot. No significant difference was found in the value of  $C$  between control and Rap1\* cells ( $p = 0.626$ , unpaired t test). The value of  $k$  was nearly 2-fold smaller in Rap1\* cells ( $p < 0.01$ , unpaired t test), indicative of a reduced rate of chromosome gathering. Scale bars represent 20  $\mu\text{m}$ .

See also Figure S2.

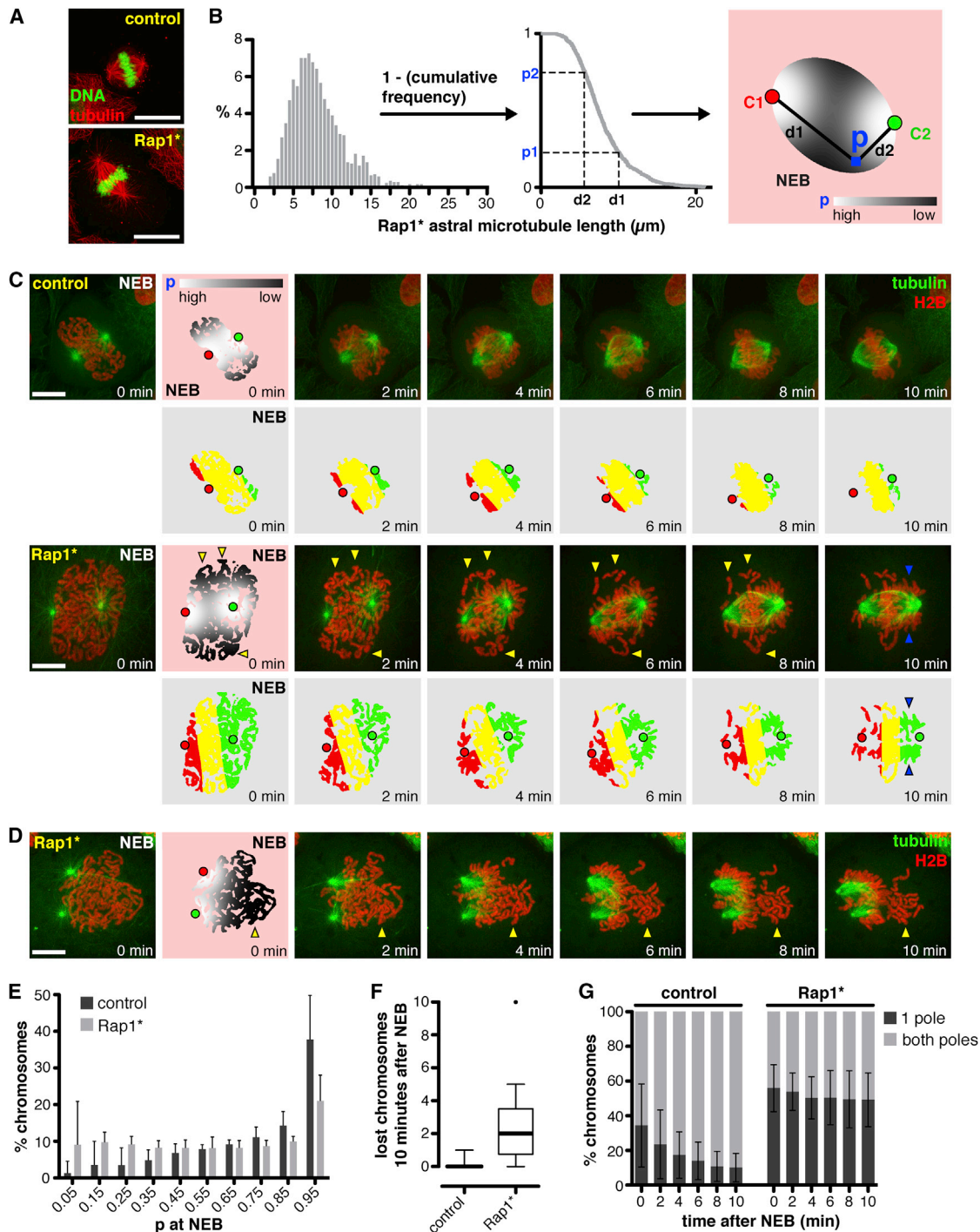


**Figure 3. Chromosomal Capture Is Limited by the Reach of Astral Microtubules**

(A) Astral microtubules in fixed control and Rap1<sup>+</sup> cells. Representative confocal images are shown as maximum projections. Scale bars represent 20 μm. (B) We calculated the probability (p) of a chromosome falling within range of a microtubule, as represented in this schematic diagram (for details see [Experimental Procedures](#)).

(C) The first stages of spindle formation in control and Rap1<sup>+</sup>-expressing HeLa cells are shown as maximum projection images. Scale bars represent 10 μm. The probability of chromosomes being within range of a microtubule at NEB was mapped onto chromosomes as a grayscale image (pink panels). The darkest regions predict chromosome loss (yellow arrows). These probabilities were then considered independently for both centrosomes (gray panels). Chromosomes within range of one centrosome became arrayed around the centrosome and along the side of the forming spindle (blue arrows).

(D) Rap1<sup>+</sup>-expressing cell in which centrosomes were located on the same side of the nucleus at NEB; many chromosomes were predicted to be lost from the nascent spindle (yellow arrows). Scale bar is 10 μm.

(E) Percentage of chromosomes with a given probability (p) of being within range of a microtubule at NEB for control (n = 10) and Rap1<sup>+</sup> (n = 8) cells.

(legend continued on next page)

data suggest that the mitotic actin cytoskeleton is dispensable for timely spindle assembly and mitotic progression in a rounded HeLa cell.

Previous studies revealed a role for the actin cortex and actomyosin-driven cortical flow in guiding centrosome separation during the early phases of mitosis (Rosenblatt et al., 2004). This is an important prerequisite for bipolar spindle assembly. However, this process does not absolutely require an actin cortex and is also driven by forces generated via microtubule sliding (Tanenbaum and Medema, 2010). Consistent with this, when we tracked centrosome position in HeLa cells expressing tubulin-GFP, we found that an increased proportion of lat-B-treated cells relative to the control failed to separate their centrosomes by the time of NEB (Figure S6A). However, lat-B-treated cells were able to assemble bipolar spindles to complete mitosis on schedule. This was not the case for cells treated with *MAD2* siRNAs, which lack a SAC and have an accelerated passage through mitosis (Figure S6B; Meraldi et al., 2004). In this situation, cells required an intact actin cortex to segregate their chromosomes (Figure S6C), consistent with their failure to undergo timely centrosome separation. Thus, although the actin-based cortex aids timely centrosome separation at the onset of mitosis and is critical in cells forced to move quickly into anaphase, this process has little impact on the overall timing of normal mitosis in HeLa cells, where progression into anaphase is dominated by the time taken to generate kinetochore/microtubule attachments that can satisfy the SAC.

Although HeLa cells dividing without external physical constraints do not require an intact actin cortex to assemble a spindle, it was not clear whether this would be the case for cells dividing in confined conditions similar to those experienced by cells dividing in a tissue (Zajac and Discher, 2008). To investigate this issue, we recorded cell division under four conditions: with or without an intact actin cytoskeleton, and in the presence or absence of a covering gel (Figure 6D). A gel stiffness of 15 kPa was chosen to mimic a tissue by being soft enough to allow division without significant defects in spindle architecture, but stiff enough to require the full force of cell rounding to deform it. Although few mitotic defects were observed in control cells as they rounded under the 15 kPa gel (Figure 6E), >80% of the flattened cells treated with cytochalasin D failed to undergo a normal mitosis. As was seen under conditions of confinement, many exhibited multipolar spindles (Figures 6E and S6D). Similarly, a large increase in multipolar spindles and cell death was observed when cells growing under 15 kPa gels were treated with lat B (Figure S6E). Thus, the actin cortex plays a minor role in the division of cells in isolation but is essential for their passage through mitosis when they are growing under conditions of physical confinement. In this context, the forces generated by the actin cortex enable cells to sustain an increase in internal cell pressure during mitosis onset, forcing the cell to round to generate enough space for spindle assembly while maintaining cell integrity (Figure 7).

## DISCUSSION

Using complementary genetic and physical approaches, we have identified an important role for mitotic cell rounding in timely chromosome capture and bipolar spindle pole stability (Figure 7). A major function of the mitotic actin cytoskeleton is therefore likely to be its contribution to mitotic rounding (Kunda and Baum, 2009). Nevertheless, studies in several systems have suggested a more direct role for the actin cytoskeleton in spindle formation (reviewed in Sandquist et al., 2011), based on observed defects in spindle morphogenesis following perturbations that altered the mitotic actin cytoskeleton (Moulding et al., 2007; Kaji et al., 2008; Kunda et al., 2008; Carreno et al., 2008) and on actin structures seen within the spindle itself (Robinson and Snyder, 2005; Fabian and Forer, 2005; Woolner et al., 2008; Vilmos et al., 2009). Further, dynein-dependent astral microtubule interactions with the actin cortex promote stable spindle orientation (Hill and Strome, 1988; Severson and Bowerman, 2003; Kaji et al., 2008; Toyoshima and Nishida, 2007; reviewed in Kunda and Baum, 2009; Morin and Bellaïche, 2011). These contacts, which are likely established at mitosis onset, are also thought to aid centrosome separation through myosin-driven cortical flow (Rosenblatt et al., 2004) and later extracentrosome clustering (Kwon et al., 2008). Finally, a circulating subcortical pool of Arp2/3-dependent actin filaments has been identified that may help to guide orientation of the metaphase spindle (Mitsushima et al., 2010; Fink et al., 2011).

Conversely, it is clear that well-formed bipolar spindles can be generated in cytoplasmic extracts devoid of actin filaments (Heald et al., 1996; Wilbur and Heald, 2013). In line with this, for isolated HeLa cells in culture, we showed that loss of the mitotic actin cortex had little impact on the overall timing of mitosis or on spindle bipolarity, in spite of the previously identified requirement for the cortex in centrosome separation operating in these cells (Rosenblatt et al., 2004). These data argue against actin performing a vital function in the heart of the mitotic spindle. However, in our experiments, the actin cortex was critically required in HeLa cells entering mitosis under a deformable gel (mimicking the mechanical environment of cells growing in a crowded tissue environment), to translate osmotic forces (Stewart et al., 2011) into the effective upward pressure required to round up. This failure to round in the presence of actin inhibitors led to profound spindle assembly defects. Cells rounding under extreme confinement also frequently exhibited significant blebbing (Figure S4B) similar to what was previously seen in mitotic *Drosophila* cells lacking an effective link between the cortex and the cell membrane (Kunda et al., 2008). These data point to an additional role for the metaphase actin cortex in stiffening the plasma membrane so that any increase in osmotic pressure leads to uniform, stable cell swelling. Although it will be important in future work to determine the roles of the mitotic actin cytoskeleton in a range of other cell types, including primary cells, this analysis suggests that many of the defects in spindle formation

(F) Numbers of chromosomes lost from the nascent spindle 10 min after NEB in control ( $n = 10$ ) and Rap1\*-expressing ( $n = 10$ ) cells. Rap1\* cells exhibited a significant increase in the number of lost chromosomes ( $p < 0.05$ , unpaired  $t$  test).

(G) Percentage of chromosomes within range of microtubules from one or both poles at progressive time points after NEB for control ( $n = 6$ ) and Rap1\*-expressing ( $n = 6$ ) cells. Graphs in (E) and (G) show mean values and error bars represent SD from the mean.

See also Figure S3.

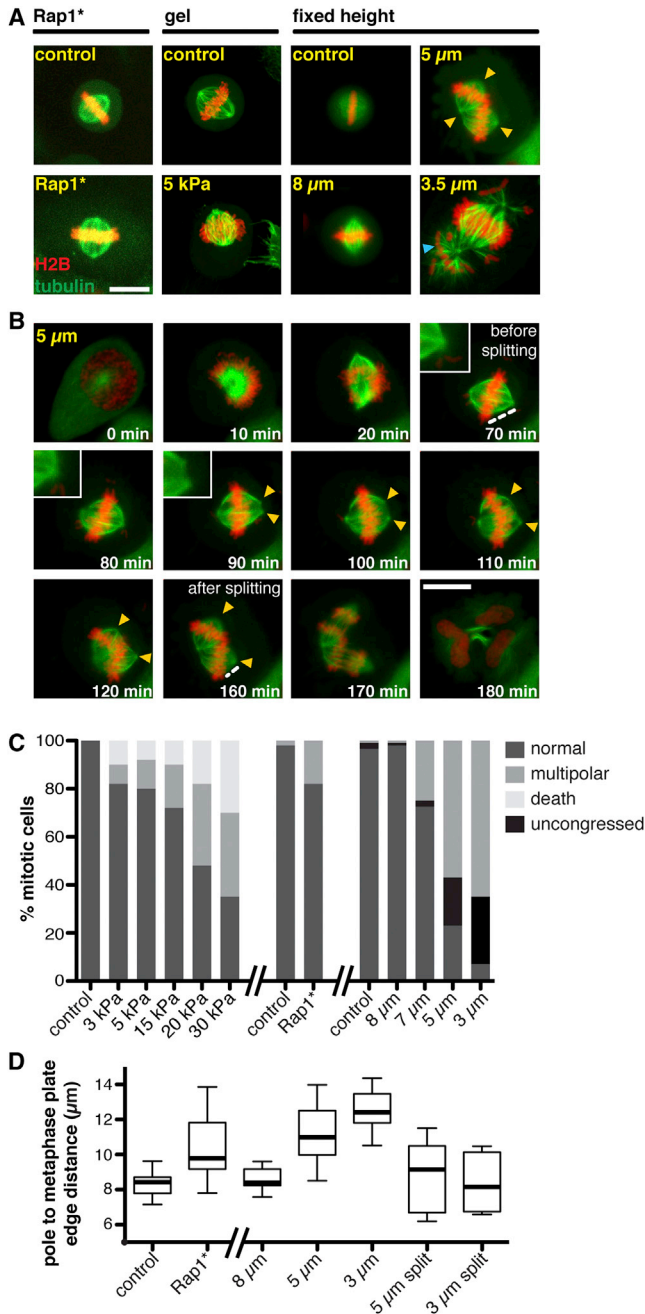


**Figure 4. Confinement in Height Leads to Pole Splitting**

(A) Images show representative mitotic spindles in control cells, in flattened cells expressing Rap1\*, in cells grown under a 5 kPa gel, or under fixed confinement. Scale bar represents 20  $\mu\text{m}$ . At high levels of confinement (5 and 3.5  $\mu\text{m}$ ), multipolar spindles (yellow arrows) and spindles with numerous uncongressed chromosomes (blue arrow) were observed.

(B) Time-lapse images of mitotic HeLa cells under 5  $\mu\text{m}$  confinement (see also Movie S3). A magnified view of the splitting pole is shown in the insets and the yellow arrows indicate the new poles formed after splitting. The dashed white lines represent pole-to-chromosome distances measured in (D). Scale bar represents 20  $\mu\text{m}$ .

(C) Defects in spindle architecture were quantified ( $n = 100, 25, 100, 45, 35, 22, 81, 43, 84, 163, 160, 51, 15$ ).

(D) Data showing the distances from the spindle pole to the edge of the metaphase plate in control and Rap1\*-expressing cells, in cells at 8  $\mu\text{m}$

associated in the literature with perturbations of the actin cortex (Fujibuchi et al., 2005; Kaji et al., 2008; Fink et al., 2011; Kunda et al., 2008; Carreno et al., 2008; Luxenburg et al., 2011) likely reflect the indirect consequences of defects in mitotic cell shape.

Why is mitotic cell shape important? Our analysis supports two distinct roles for cell geometry in efficient spindle morphogenesis, both of which are related to the limited reach of microtubules in mitotic cells (Collins et al., 2012; Domnitz et al., 2012). First, cell rounding limits the space that microtubules have to search (Kirschner and Mitchison, 1986), bringing the chromosomes released upon NEB into an optimal range for the rapid establishment of microtubule-kinetochore contacts. Previous work has hinted at the limited efficiency of unaided search and capture in the context of normal rounded cells (Wollman et al., 2005; Magidson et al., 2011). In flattened cells, the altered geometric arrangement of chromosomes and microtubules results in profound problems in spindle assembly (Figure 7, d). It takes time to correct these early errors, likely making flattened cells reliant on chromosome-associated microtubule motors (e.g., CENP-E) whose function may be less critical in a normal mitosis (Kapoor et al., 2006; Kim et al., 2010). Interestingly, similar paths of spindle assembly have been observed in cell lines that exhibit a flattened geometry during normal passage through mitosis (e.g., PtK1 cells and newt pneumocytes; Hayden et al., 1990; Roos, 1976; Rieder and Alexander, 1990), emphasizing the importance of considering cell geometry when studying spindle assembly.

Geometric constraints on chromosome capture are even greater in other systems. For example, in large cells, such as those seen during early metazoan development, spindles often fail to scale with cell size (Wühr et al., 2008). As a result, efficient chromosome capture must rely on additional mechanisms. In *Drosophila* oocytes, for example, meiotic chromosomes are clustered in a structure called the karyosome, around which the spindle assembles (Cullen et al., 2005; Lancaster et al., 2007). And in starfish oocytes, an actin filament network surrounding meiotic chromosomes brings chromosomes within range of the limited reach of spindle microtubules (Lénárt et al., 2005). Of course, spindles also have to scale with changes in cell size that accompany development. Interestingly, a recent study implicated *Xenopus* importin- $\alpha$  in this process (Wilbur and Heald, 2013). Strikingly, this protein also regulates interphase nuclear size, which our analysis suggests is likely to play a critical role in determining the spread of chromosomes at NEB. These data suggest that importin- $\alpha$  levels could mechanistically couple nuclear size and spindle microtubule lengths to facilitate efficient search and capture at NEB.

Second, we have identified a role for mitotic rounding in ensuring spindle pole stability. Previous work has shown that pressing on naturally flat mitotic cells (PtK2) both widens the metaphase plate and increases spindle length (Dumont and Mitchison, 2009). Here, we extend this finding. Once the increase in spindle length that is induced by reducing the height of cells entering mitosis exceeds the reach of most mitotic microtubules,

confinement, and in cells at 5 and 3  $\mu\text{m}$  confinement before and after pole splitting ( $n = 18, 18, 19, 17, 13, 9, 4$ ).

See also Figure S4.

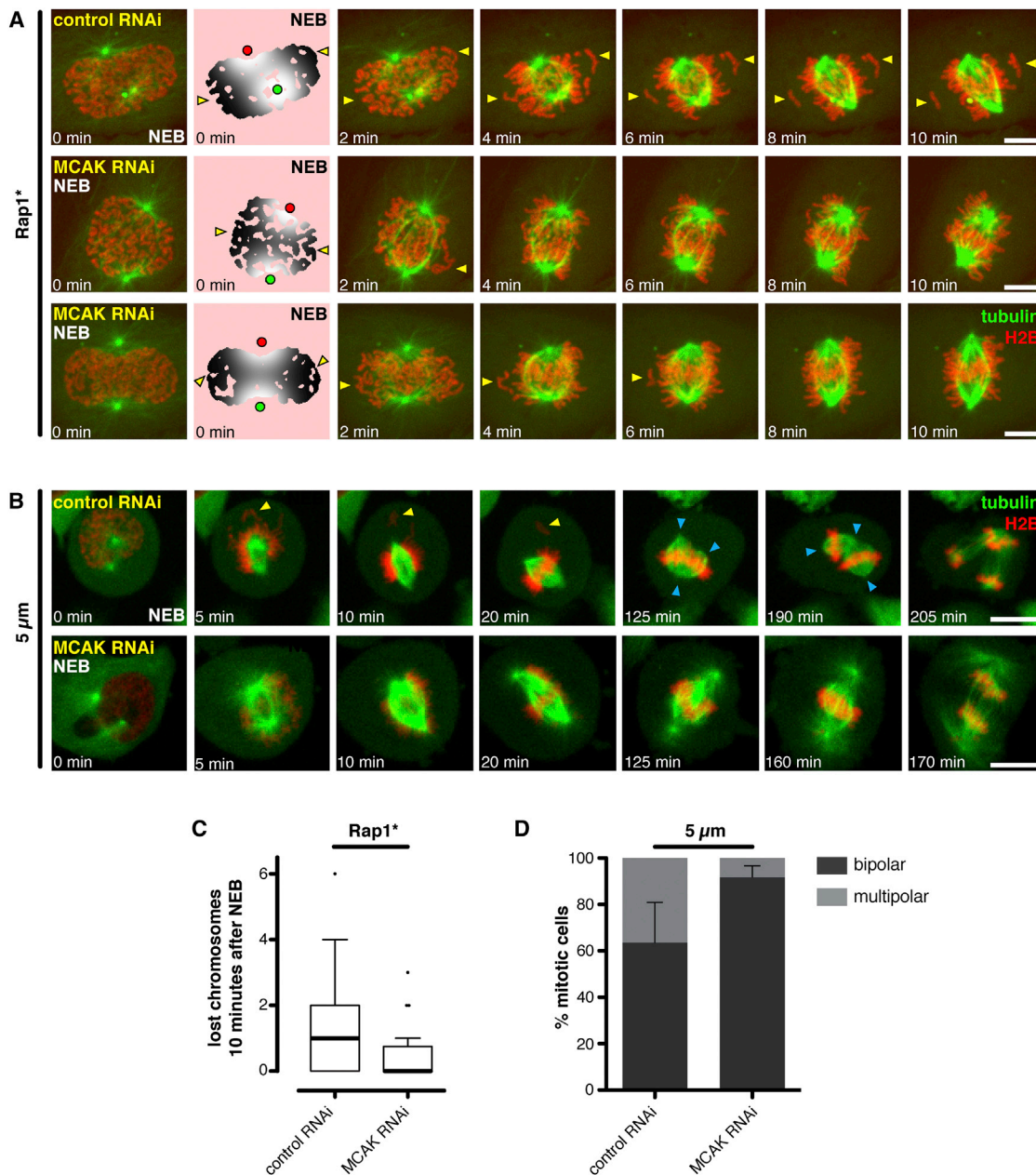


**Figure 5. Rescuing Mitotic Defects in Flat Cells by Increasing Microtubule Lengths**

(A) Representative maximum projection time-lapse images of the first stages of spindle formation in control and MCAK-depleted HeLa cells expressing Rap1\*. The probability of chromosomes being within range of a microtubule at NEB was calculated as shown in Figure 3B and mapped onto the chromosomes as a grayscale image (pink panels). The darkest regions predict chromosome loss in control depleted cells (top panel). Distant chromosomes (yellow arrows) were successfully captured in MCAK-depleted cells (bottom panels). Scale bar represents 10  $\mu$ m.

(B) Representative time-lapse images of control and MCAK-depleted cells growing under 5  $\mu$ m confinement. Lost chromosomes were observed during early stages of spindle formation (yellow arrow) in control depleted cells but not in cells lacking MCAK. Pole-splitting events (blue arrows) were rescued by MCAK RNAi. Scale bar represents 20  $\mu$ m.

(C) Plot showing the number of chromosomes lost from the nascent spindle 10 min after NEB in control (n = 24) and MCAK-depleted (n = 20) Rap1\* cells. Fewer chromosomes were lost from the nascent spindle in flat Rap1\*-expressing cells when microtubules were lengthened in the absence of MCAK (p < 0.05, unpaired t test).

(D) Percentage of monopolar spindles in control and MCAK-depleted cells confined in height to 5  $\mu$ m (n = 267, 342; in five experiments). Data are represented as means; error bars represent SD between experiments. Fewer multipolar spindles were observed in mitotic cells confined to 5  $\mu$ m in height when microtubules were lengthened in the absence of MCAK (p < 0.01, unpaired t test).

See also Figure S5.

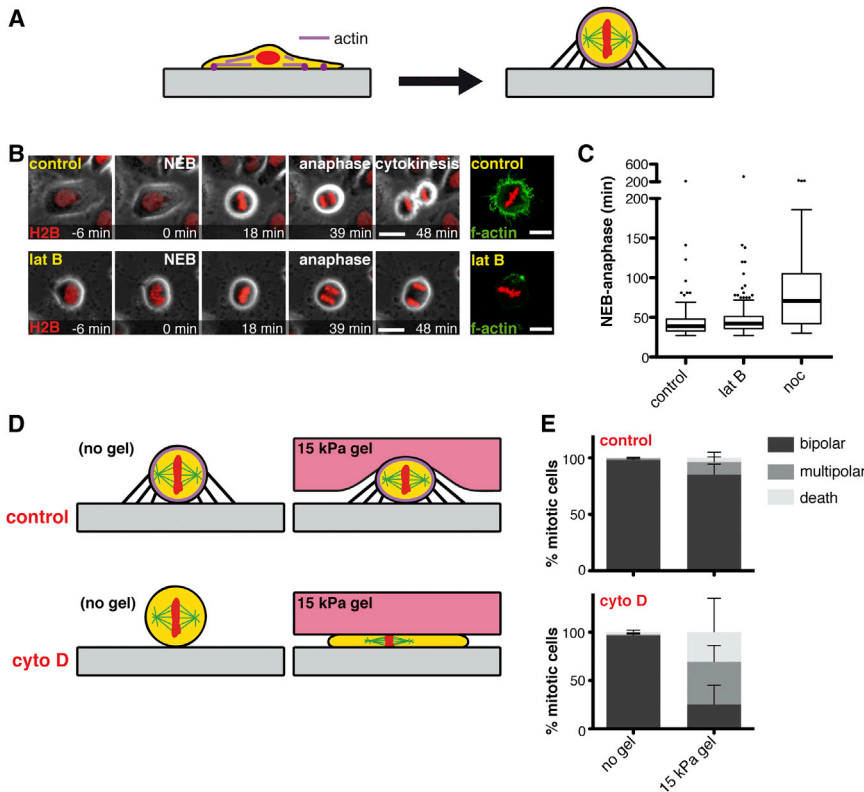


**Figure 6. F-Actin Is Only Essential for Mitosis under Conditions of Confinement**

(A) Schematic diagram showing changes in actin organization during mitosis.

(B) Time-lapse images of mitosis in control cells or cells treated with lat B (5  $\mu$ M) to induce loss of F-actin (see also [Movie S4](#)). To confirm F-actin loss, actin filaments were visualized in fixed control and lat-B-treated cells using fluorophore-labeled phalloidin. Scale bars represent 20  $\mu$ m.

(C) Plot shows NEB to anaphase timing for control cells (n = 146), lat-B-treated cells (n = 153), and cells treated with a low dose (7 ng/ml) of nocodazole (n = 128). Mitotic timing was similar in control and lat-B-treated cells (p = 0.09, unpaired t test), whereas nocodazole delayed anaphase onset (p < 0.0001, unpaired t test).

(D) Actin is required for spindle assembly in cells growing under a soft gel. Schematic diagram showing the principle of the experiment. Cells were plated on a glass slide and then grown in the presence (right column) or absence (left column) of a covering gel and treated with cytochalasin D (0.5  $\mu$ M; bottom row) or left untreated (top row).

(E) Mitotic phenotypes of HeLa cells in the four conditions described in (D) (n = 306, 679; 335, 503; in more than three experiments). Errors bars represent SD from the mean. Normal bipolar mitosis was decreased and multipolar spindles were increased in cells with a perturbed actin cortex growing under gels (p < 0.01, p < 0.05, unpaired t test, respectively).

See also [Figure S6](#).

the spindles collapse through the generation of additional acen- triolar poles (Figure 7, d<sub>2</sub>). Such multipolar figures have been seen in cells carrying extra centrosomes (Kwon et al., 2008) and in cells with specific centrosomal defects (Logarinho et al., 2012). In our case, however, multipolarity results from simple geometric constraints in the system. Importantly, pole splitting is not a consequence of the defects described at NEB. Instead, they appear at metaphase at a precise threshold in cell height: below 8  $\mu$ m. Interestingly, Rap1\*-expressing cells rarely experience this level of confinement at metaphase, because their height gradually increases following entry into mitosis and peaks at metaphase at a position coincident with the metaphase plate. In the face of counteracting membrane tension, the developing metaphase plate may therefore apply a vertical force that helps to generate the space it requires. Importantly, geometric requirements for stable bipolar spindle formation appear to be a general phenomenon, since similar defects were observed in all cell types tested (unpublished data), although to different degrees and for different height thresholds. Moreover, in a previous study (Dinarina et al., 2009), multipolar spindles were seen in spindles assembled in vitro around metaphase plates of increasing length and were linked to limited microtubule lengths.

Although our analysis of the geometric requirements of spindle formation in mitotic cells focused on the reach of microtubules, other factors will likely come into play. For example, in preventing rounding, the ring-like arrangement of prometaphase chromosomes that was previously described to facilitate efficient establishment of amphitelic chromosome attachments (Magidson et al., 2011) will be altered, likely contributing to the reduced

efficiency of chromosome capture by the nascent spindle. Importantly, spindle defects in flat mitotic cells also appear to depend on chromosome numbers. Spindle morphogenesis begins to fail at <8  $\mu$ m in near-triploid HeLa cells, <5  $\mu$ m in diploid RPE1 cells, and <3.5  $\mu$ m in PtK2 cells (unpublished data; Dumont and Mitchison, 2009). This may be why naturally flat mitotic cells have smaller numbers of chromosomes (e.g., PtK cells have six chromosomes; Torosantucci et al., 2009). Moreover, increased numbers of centrosomes make cells more sensitive to rounding defects (unpublished data). For cancer cells with high ploidy and extra centrosomes, robust actin-dependent mitotic rounding is therefore likely to be critical for the successful establishment of metastases in crowded tissue environments (Matthews and Baum, 2012). Thus, by revealing roles for cell geometry in mitotic spindle assembly and spindle bipolarity, our findings have important implications for our understanding of normal and cancer cell divisions in isolation and in a tissue context.

## EXPERIMENTAL PROCEDURES

### Cell Culture, DNA Transfection, RNAi, Immunoblotting, and Drug Treatments

Unlabeled HeLa Kyoto cells and HeLa stable cell lines expressing LifeAct-GFP/H2B-mRFP (Matthews et al., 2012), H2B-mRFP/tubulin-GFP (Steigemann et al., 2009), or H2B-mRFP/myrPalm-GFP were cultured under standard conditions.

HeLa cells were transfected with *pRK5-Rap1[Q63E]* (Rap1\*; Dao et al., 2009) using Fugene HD (Roche) according to the manufacturer's instructions. Control transfection reactions were performed in the absence of plasmid DNA. Cells transfected with Rap1\* were identified by their failure to round up in

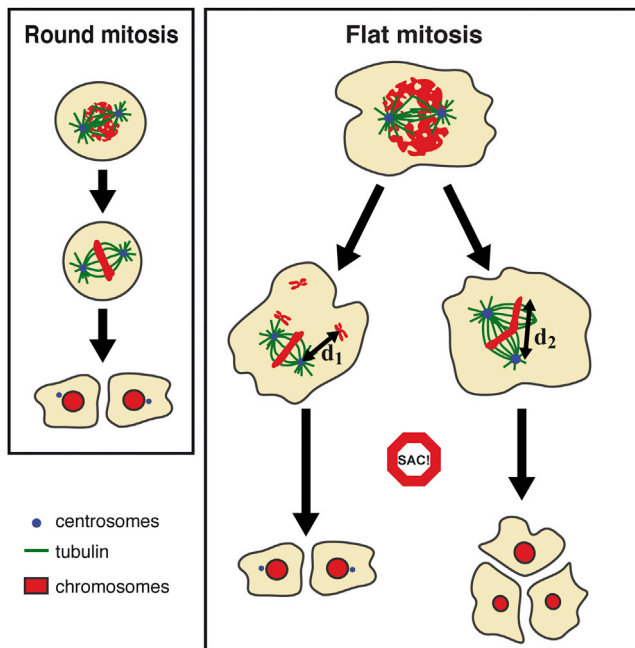


**Figure 7. A Model for the Role of Cell Geometry in Mitosis**

Schematic diagram summarizing the consequences of mitotic cell rounding defects for mitotic spindle formation.

mitosis. HeLa cells were transfected with siRNAs using Lipofectamine 2000 or RNAiMAX (Invitrogen) as previously described (Rohn et al., 2011). Depletion of MCAK was verified by immunoblotting as previously described (Matthews et al., 2012), using a specific MCAK antibody (mouse monoclonal IG2; Abnova). Since both siRNAs tested reduced MCAK protein levels to similar extents, siRNA2 was used in all experiments. Cells were treated with 5  $\mu$ M latrunculin B (Calbiochem), 0.5  $\mu$ M cytochalasin D, 7 ng/ml nocodazole (Sigma), and 5  $\mu$ M S-trityl-L-cysteine (STLC; Sigma), and, where indicated, control treatments were performed with an equivalent volume of the solvent DMSO. Methods are detailed in Supplemental Experimental Procedures.

#### Micropatterning

Micropatterned islands of fibronectin together with Alexa Fluor 405 IgG (Invitrogen) were fabricated on glass-bottomed dishes (MatTek; see Supplemental Experimental Procedures). HeLa cells expressing Rap1\* were trypsinized (using Trypsin-EDTA; Invitrogen), resuspended in medium at a density of 60,000 cells/ml, seeded onto micropatterned glass-bottomed dishes, and incubated at 37°C under 5% CO<sub>2</sub> for 1 hr. After 1 hr, the cells were washed in fresh medium and incubated for 4 hr to allow spreading on patterned fibronectin before they were processed for microscopy.

#### Gels and Confinement

Polyacrylamide gel layers (1 mm thick) of different rigidities were attached to 18-mm-diameter glass coverslips (see Supplemental Experimental Procedures). Cells were seeded at 3,000 cells/cm<sup>2</sup> in 12-well plates before glass slides holding the gels were fixed onto a modified six-well plate cover, allowing them to be gently positioned onto cells, as previously described (Le Berre et al., 2012). For confocal microscopy, a cell confiner (described below) was used to handle 10-mm-diameter gel-covered coverslips on glass-bottomed dishes.

For confinement assays, cells were seeded at 3,000 cells/cm<sup>2</sup> in 35 mm glass-bottomed dishes (Fluorodish; ITW) coated with a 25  $\mu$ g/ml fibronectin solution. The next day, the cells were confined in a defined space (3.5–8  $\mu$ m) as previously described (Le Berre et al., 2012; see Supplemental Experimental Procedures). Briefly, micropillar spacers of the desired height were molded

onto a thin layer of PDMS coating 10-mm-diameter glass coverslips. A precision vacuum controller (VG1006; Elveflow) operating a custom-made suction cup device gently positioned the textured slide onto the cells, confining the cells with submicrometer homogeneity.

#### Live-Cell Microscopy and Immunofluorescence

For live-cell imaging, cells were seeded on glass-bottomed dishes (MatTek) coated with 10  $\mu$ g/ml fibronectin (Sigma), on micropatterned fibronectin, under gels or under PDMS. For mitotic timing experiments, cells were imaged every 2, 3, or 5 min. Details are described in Supplemental Experimental Procedures.

For immunofluorescence, cells on fibronectin-coated glass coverslips were fixed with 4% formaldehyde (TAAB), permeabilized with 0.5% Triton X-100 (Sigma) in PBS for 5 min, and blocked with 5% bovine serum albumin (Sigma) in PBS for 30 min. The cells were sequentially incubated with primary and fluorescently labeled secondary antibodies for 1 hr at room temperature and then washed in PBS, 0.1% Triton X-100. The cells were mounted in FluorSave (Calbiochem) and images were acquired using a Leica TCS SPE laser scanning confocal microscope system. The antibodies used in immunofluorescence are listed in Supplemental Experimental Procedures.

#### Image Processing and Analysis

Displayed images were processed using ImageJ, and, where necessary, contrast/brightness was changed uniformly across the field.

To measure cell length and height, the x, y, and z scales of microscopes were calibrated using 19.28  $\pm$  0.3  $\mu$ m beads coated with fluorescent PII-g-PEG (SuSoS) by soaking for 30 min in a 0.5 mg/ml PLL-g-PEG solution in 10 mM HEPES pH 7.4 after plasma activation. The scale indicating cell height in Figure 1H was calculated using a mechanical model in which cells under gels were assumed to be half a sphere having the same volume as a normally round mitotic cell (a sphere of 20  $\mu$ m diameter). A detailed description of this mechanical model can be found in Supplemental Experimental Procedures.

Image analyses of chromosome congression (Figure 2), astral microtubule lengths (Figures 3 and S3), and chromosome capture (Figures 3 and 5) were performed using custom MATLAB scripts; see Supplemental Experimental Procedures for details.

#### Statistical Analysis

Prism software (GraphPad) was used to generate graphs and for the statistical analysis. Box plots show median, upper, and lower quartiles as the box, whiskers represent 1.5 times the interquartile distance, and the remaining points are shown as outliers. All data points were included in statistical analyses. All remaining graphs are described in the figure legends, alongside statistical tests and associated p values.

#### SUPPLEMENTAL INFORMATION

Supplemental Information includes six figures, four movies, and Supplemental Experimental Procedures and can be found with this article online at <http://dx.doi.org/10.1016/j.devcel.2013.03.014>.

#### ACKNOWLEDGMENTS

We thank Roie Shlomovitz for inspiration early in the course of this work and Thomas Surrey, Sarah Woolner, Alexey Khodjakov, and members of the Baum and Piel groups for critical readings of the manuscript. This work was supported by Cancer Research UK (B.B. and O.M.L.), the EU Cancer Pathways Project (O.M.L.), CoMPLEX (A.D. and R.P.), Vivattech and the Fondation ARC pour la Recherche sur le Cancer (M.L.B.), Ligue contre le Cancer (M.P.), and INCA grant 2011-1-PLBIO-11-IC-1 (M.P. and B.B.). We would also like to express our sadness at the loss of our coauthor Tom Duke several months before the completion of this project.

Received: November 12, 2012

Revised: February 14, 2013

Accepted: March 21, 2013

Published: April 25, 2013

## REFERENCES

- Carreno, S., Kouranti, I., Glusman, E.S., Fuller, M.T., Echard, A., and Payre, F. (2008). Moesin and its activating kinase Slik are required for cortical stability and microtubule organization in mitotic cells. *J. Cell Biol.* *180*, 739–746.
- Collins, E.S., Balchand, S.K., Faraci, J.L., Wadsworth, P., and Lee, W.L. (2012). Cell cycle-regulated cortical dynein/dynactin promotes symmetric cell division by differential pole motion in anaphase. *Mol. Biol. Cell* *23*, 3380–3390.
- Cramer, L.P., and Mitchison, T.J. (1997). Investigation of the mechanism of retraction of the cell margin and rearward flow of nodules during mitotic cell rounding. *Mol. Biol. Cell* *8*, 109–119.
- Cullen, C.F., Brittle, A.L., Ito, T., and Ohkura, H. (2005). The conserved kinase NHK-1 is essential for mitotic progression and unifying acentrosomal meiotic spindles in *Drosophila melanogaster*. *J. Cell Biol.* *171*, 593–602.
- Dao, V.T., Dupuy, A.G., Gavet, O., Caron, E., and de Gunzburg, J. (2009). Dynamic changes in Rap1 activity are required for cell retraction and spreading during mitosis. *J. Cell Sci.* *122*, 2996–3004.
- Dinarina, A., Pugieux, C., Corral, M.M., Loose, M., Spatz, J., Karsenti, E., and Nédélec, F. (2009). Chromatin shapes the mitotic spindle. *Cell* *138*, 502–513.
- Domnitz, S.B., Wagenbach, M., Decarreau, J., and Wordeman, L. (2012). MCAK activity at microtubule tips regulates spindle microtubule length to promote robust kinetochore attachment. *J. Cell Biol.* *197*, 231–237.
- Dumont, S., and Mitchison, T.J. (2009). Compression regulates mitotic spindle length by a mechanochemical switch at the poles. *Curr. Biol.* *19*, 1086–1095.
- Fabian, L., and Forer, A. (2005). Redundant mechanisms for anaphase chromosome movements: crane-fly spermatocyte spindles normally use actin filaments but also can function without them. *Protoplasma* *225*, 169–184.
- Fededa, J.P., and Gerlich, D.W. (2012). Molecular control of animal cell cytokinesis. *Nat. Cell Biol.* *14*, 440–447.
- Fink, J., Carpi, N., Betz, T., Bétard, A., Chebah, M., Azioune, A., Bornens, M., Sykes, C., Fetler, L., Cuvelier, D., and Piel, M. (2011). External forces control mitotic spindle positioning. *Nat. Cell Biol.* *13*, 771–778.
- Fujibuchi, T., Abe, Y., Takeuchi, T., Imai, Y., Kamei, Y., Murase, R., Ueda, N., Shigemoto, K., Yamamoto, H., and Kito, K. (2005). AIP1/WDR1 supports mitotic cell rounding. *Biochem. Biophys. Res. Commun.* *327*, 268–275.
- Gibson, W.T., Veldhuis, J.H., Rubinstein, B., Cartwright, H.N., Perrimon, N., Brodland, G.W., Nagpal, R., and Gibson, M.C. (2011). Control of the mitotic cleavage plane by local epithelial topology. *Cell* *144*, 427–438.
- Hayden, J.H., Bowser, S.S., and Rieder, C.L. (1990). Kinetochores capture astral microtubules during chromosome attachment to the mitotic spindle: direct visualization in live newt lung cells. *J. Cell Biol.* *111*, 1039–1045.
- Heald, R., Tournebise, R., Blank, T., Sandaltzopoulos, R., Becker, P., Hyman, A., and Karsenti, E. (1996). Self-organization of microtubules into bipolar spindles around artificial chromosomes in *Xenopus* egg extracts. *Nature* *382*, 420–425.
- Hill, D.P., and Strome, S. (1988). An analysis of the role of microfilaments in the establishment and maintenance of asymmetry in *Caenorhabditis elegans* zygotes. *Dev. Biol.* *125*, 75–84.
- Kaji, N., Muramoto, A., and Mizuno, K. (2008). LIM kinase-mediated cofilin phosphorylation during mitosis is required for precise spindle positioning. *J. Biol. Chem.* *283*, 4983–4992.
- Kapoor, T.M., Lampson, M.A., Hergert, P., Cameron, L., Cimini, D., Salmon, E.D., McEwen, B.F., and Khodjakov, A. (2006). Chromosomes can congress to the metaphase plate before biorientation. *Science* *311*, 388–391.
- Kim, Y., Holland, A.J., Lan, W., and Cleveland, D.W. (2010). Aurora kinases and protein phosphatase 1 mediate chromosome congression through regulation of CENP-E. *Cell* *142*, 444–455.
- Kirschner, M., and Mitchison, T. (1986). Beyond self-assembly: from microtubules to morphogenesis. *Cell* *45*, 329–342.
- Kunda, P., and Baum, B. (2009). The actin cytoskeleton in spindle assembly and positioning. *Trends Cell Biol.* *19*, 174–179.
- Kunda, P., Pelling, A.E., Liu, T., and Baum, B. (2008). Moesin controls cortical rigidity, cell rounding, and spindle morphogenesis during mitosis. *Curr. Biol.* *18*, 91–101.
- Kunda, P., Rodrigues, N.T., Moeendarbary, E., Liu, T., Ivetic, A., Charras, G., and Baum, B. (2012). PP1-mediated moesin dephosphorylation couples polar relaxation to mitotic exit. *Curr. Biol.* *22*, 231–236.
- Kwon, M., Godinho, S.A., Chandhok, N.S., Ganem, N.J., Azioune, A., Thery, M., and Pellman, D. (2008). Mechanisms to suppress multipolar divisions in cancer cells with extra centrosomes. *Genes Dev.* *22*, 2189–2203.
- Lancaster, O.M., Cullen, C.F., and Ohkura, H. (2007). NHK-1 phosphorylates BAF to allow karyosome formation in the *Drosophila* oocyte nucleus. *J. Cell Biol.* *179*, 817–824.
- Lara-Gonzalez, P., Westhorpe, F.G., and Taylor, S.S. (2012). The spindle assembly checkpoint. *Curr. Biol.* *22*, R966–R980.
- Le Berre, M., Aubertin, J., and Piel, M. (2012). Fine control of nuclear confinement identifies a threshold deformation leading to lamina rupture and induction of specific genes. *Integr. Biol. (Camb)* *4*, 1406–1414.
- Lénárt, P., Bacher, C.P., Daigle, N., Hand, A.R., Eils, R., Terasaki, M., and Ellenberg, J. (2005). A contractile nuclear actin network drives chromosome congression in oocytes. *Nature* *436*, 812–818.
- Logarinho, E., Maffini, S., Barisic, M., Marques, A., Toso, A., Meraldi, P., and Maiato, H. (2012). CLASPs prevent irreversible multipolarity by ensuring spindle-pole resistance to traction forces during chromosome alignment. *Nat. Cell Biol.* *14*, 295–303.
- Luxenburg, C., Pasolli, H.A., Williams, S.E., and Fuchs, E. (2011). Developmental roles for Srf, cortical cytoskeleton and cell shape in epidermal spindle orientation. *Nat. Cell Biol.* *13*, 203–214.
- Maddox, A.S., and Burridge, K. (2003). RhoA is required for cortical retraction and rigidity during mitotic cell rounding. *J. Cell Biol.* *160*, 255–265.
- Magidson, V., O'Connell, C.B., Loncarek, J., Paul, R., Mogilner, A., and Khodjakov, A. (2011). The spatial arrangement of chromosomes during prometaphase facilitates spindle assembly. *Cell* *146*, 555–567.
- Matthews, H.K., and Baum, B. (2012). The metastatic cancer cell cortex: an adaptation to enhance robust cell division in novel environments? *Bioessays* *34*, 1017–1020.
- Matthews, H.K., Delabre, U., Rohn, J.L., Guck, J., Kunda, P., and Baum, B. (2012). Changes in Ect2 localization couple actomyosin-dependent cell shape changes to mitotic progression. *Dev. Cell* *23*, 371–383.
- Meraldi, P., Draviam, V.M., and Sorger, P.K. (2004). Timing and checkpoints in the regulation of mitotic progression. *Dev. Cell* *7*, 45–60.
- Mitsushima, M., Aoki, K., Ebisuya, M., Matsumura, S., Yamamoto, T., Matsuda, M., Toyoshima, F., and Nishida, E. (2010). Revolving movement of a dynamic cluster of actin filaments during mitosis. *J. Cell Biol.* *191*, 453–462.
- Morin, X., and Bellaïche, Y. (2011). Mitotic spindle orientation in asymmetric and symmetric cell divisions during animal development. *Dev. Cell* *21*, 102–119.
- Moulding, D.A., Blundell, M.P., Spiller, D.G., White, M.R., Cory, G.O., Calle, Y., Kempski, H., Sinclair, J., Ancliff, P.J., Kinnon, C., et al. (2007). Unregulated actin polymerization by WASp causes defects of mitosis and cytokinesis in X-linked neutropenia. *J. Exp. Med.* *204*, 2213–2224.
- Musacchio, A. (2011). Spindle assembly checkpoint: the third decade. *Philos. Trans. R. Soc. Lond. B Biol. Sci.* *366*, 3595–3604.
- O'Connell, C.B., Loncarek, J., Hergert, P., Kourtidis, A., Conklin, D.S., and Khodjakov, A. (2008). The spindle assembly checkpoint is satisfied in the absence of interkinetochore tension during mitosis with unreplicated genomes. *J. Cell Biol.* *183*, 29–36.
- Picone, R., Ren, X., Ivanovitch, K.D., Clarke, J.D., McKendry, R.A., and Baum, B. (2010). A polarised population of dynamic microtubules mediates homeostatic length control in animal cells. *PLoS Biol.* *8*, e1000542.
- Piehl, M., and Cassimeris, L. (2003). Organization and dynamics of growing microtubule plus ends during early mitosis. *Mol. Biol. Cell* *14*, 916–925.

- Rieder, C.L., and Alexander, S.P. (1990). Kinetochores are transported poleward along a single astral microtubule during chromosome attachment to the spindle in newt lung cells. *J. Cell Biol.* 110, 81–95.
- Robinson, R.W., and Snyder, J.A. (2005). Localization of myosin II to chromosome arms and spindle fibers in PtK1 cells: a possible role for an actomyosin system in mitosis. *Protoplasma* 225, 113–122.
- Rohn, J.L., Sims, D., Liu, T., Fedorova, M., Schöck, F., Dopie, J., Vartiainen, M.K., Kiger, A.A., Perrimon, N., and Baum, B. (2011). Comparative RNAi screening identifies a conserved core metazoan actinome by phenotype. *J. Cell Biol.* 194, 789–805.
- Roos, U.P. (1976). Light and electron microscopy of rat kangaroo cells in mitosis. III. Patterns of chromosome behavior during prometaphase. *Chromosoma* 54, 363–385.
- Rosenblatt, J., Cramer, L.P., Baum, B., and McGee, K.M. (2004). Myosin II-dependent cortical movement is required for centrosome separation and positioning during mitotic spindle assembly. *Cell* 117, 361–372.
- Sandquist, J.C., Kita, A.M., and Bement, W.M. (2011). And the dead shall rise: actin and myosin return to the spindle. *Dev. Cell* 21, 410–419.
- Sedzinski, J., Biro, M., Oswald, A., Tinevez, J.Y., Salbreux, G., and Paluch, E. (2011). Polar actomyosin contractility destabilizes the position of the cytokinetic furrow. *Nature* 476, 462–466.
- Severson, A.F., and Bowerman, B. (2003). Myosin and the PAR proteins polarize microfilament-dependent forces that shape and position mitotic spindles in *Caenorhabditis elegans*. *J. Cell Biol.* 161, 21–26.
- Skoufias, D.A., Andreassen, P.R., Lacroix, F.B., Wilson, L., and Margolis, R.L. (2001). Mammalian mad2 and bub1/bubR1 recognize distinct spindle-attachment and kinetochore-tension checkpoints. *Proc. Natl. Acad. Sci. USA* 98, 4492–4497.
- Steigemann, P., Wurzenberger, C., Schmitz, M.H., Held, M., Guizetti, J., Maar, S., and Gerlich, D.W. (2009). Aurora B-mediated abscission checkpoint protects against tetraploidization. *Cell* 136, 473–484.
- Stewart, M.P., Helenius, J., Toyoda, Y., Ramanathan, S.P., Muller, D.J., and Hyman, A.A. (2011). Hydrostatic pressure and the actomyosin cortex drive mitotic cell rounding. *Nature* 469, 226–230.
- Tanenbaum, M.E., and Medema, R.H. (2010). Mechanisms of centrosome separation and bipolar spindle assembly. *Dev. Cell* 19, 797–806.
- Torosantucci, L., De Santis Puzzon, M., Cenciarelli, C., Rens, W., and Degrossi, F. (2009). Aneuploidy in mitosis of PtK1 cells is generated by random loss and nondisjunction of individual chromosomes. *J. Cell Sci.* 122, 3455–3461.
- Toyoshima, F., and Nishida, E. (2007). Integrin-mediated adhesion orients the spindle parallel to the substratum in an EB1- and myosin X-dependent manner. *EMBO J.* 26, 1487–1498.
- Tse, H.T., Weaver, W.M., and Di Carlo, D. (2012). Increased asymmetric and multi-daughter cell division in mechanically confined microenvironments. *PLoS ONE* 7, e38986.
- Uchida, K.S., Takagaki, K., Kumada, K., Hirayama, Y., Noda, T., and Hirota, T. (2009). Kinetochore stretching inactivates the spindle assembly checkpoint. *J. Cell Biol.* 184, 383–390.
- Varga, V., Leduc, C., Bormuth, V., Diez, S., and Howard, J. (2009). Kinesin-8 motors act cooperatively to mediate length-dependent microtubule depolymerization. *Cell* 138, 1174–1183.
- Vilmos, P., Jankovics, F., Szathmári, M., Lukácsovich, T., Henn, L., and Erdélyi, M. (2009). Live imaging reveals that the *Drosophila* actin-binding ERM protein, moesin, co-localizes with the mitotic spindle. *Eur. J. Cell Biol.* 88, 609–619.
- Walczak, C.E., and Heald, R. (2008). Mechanisms of mitotic spindle assembly and function. *Int. Rev. Cytol.* 265, 111–158.
- Wilbur, J.D., and Heald, R. (2013). Mitotic spindle scaling during *Xenopus* development by kif2a and importin  $\alpha$ . *eLife* 2, e00290.
- Wollman, R., Cytrynbaum, E.N., Jones, J.T., Meyer, T., Scholey, J.M., and Mogilner, A. (2005). Efficient chromosome capture requires a bias in the 'search-and-capture' process during mitotic-spindle assembly. *Curr. Biol.* 15, 828–832.
- Woolner, S., O'Brien, L.L., Wiese, C., and Bement, W.M. (2008). Myosin-10 and actin filaments are essential for mitotic spindle function. *J. Cell Biol.* 182, 77–88.
- Wühr, M., Chen, Y., Dumont, S., Groen, A.C., Needleman, D.J., Salic, A., and Mitchison, T.J. (2008). Evidence for an upper limit to mitotic spindle length. *Curr. Biol.* 18, 1256–1261.
- Zajac, A.L., and Discher, D.E. (2008). Cell differentiation through tissue elasticity-coupled, myosin-driven remodeling. *Curr. Opin. Cell Biol.* 20, 609–615.